Nanoengineering membrane surfaces: A new paradigm for efficient CO_2 capture

Leiqing Hu*, Vinh T. Bui, Narjes Esmaeili, Haiqing Lin*

Department of Chemical and Biological Engineering, University at Buffalo, The State University of New York, Buffalo, NY 14260, USA

*Corresponding authors:

Leiqing Hu, E-mail: leiqingh@buffalo.edu

Haiqing Lin, E-mail: haiqingl@buffalo.edu

ABSTRACT

Thin-film composite (TFC) membranes with superior separation properties for H₂/CO₂, CO₂/N₂, and CO₂/CH₄ are of great interest for CO₂ capture. As the selective layer of the membranes becomes thinner (~100 nm or less) to enhance gas permeance, it can be surface-engineered to significantly improve gas separation properties. This paper aims to critically review scalable nanotechnologies adopted to modify membrane surfaces to improve CO₂ capture performance, including atomic layer deposition, chemical vapor deposition, plasma treatment, direct fluorination, ion/electron beam treatment, ozone treatment, and surface-initiated polymerization. We first describe the mechanisms of these nanotechnologies to achieve desired surface chemistries and nanostructures. Second, examples of surface-modified membranes with enhanced CO₂ capture performance are highlighted, and they are compared with state-of-the-art membranes to showcase their potential for gas separations. Finally, we summarize the pros and cons of these technologies to transform membrane technology for practical applications.

Keywords: Thin-film composite membranes, CO₂ capture, Surface modification, Atomic layer deposition, Chemical vapor deposition.

1. Introduction

The elevated CO₂ concentration in the atmosphere is widely believed to cause global climate change, and CO₂ capture from large industrial emission points such as fossil fuel- or biomass-fired power plants is a vital approach to reducing the CO₂ emissions to the atmosphere. In these processes, carbon sources (fossil fuels or biomasses) can be combusted first to produce flue gas, and CO₂/N₂ separation is needed for carbon capture (i.e., post-combustion carbon capture) (Sandru et al., 2022); carbon sources can also be decarbonized first to produce H₂ and CO₂, and H₂/CO₂ separation is needed to produce H₂ as an energy carrier and CO₂ for storage and utilization (i.e., pre-combustion carbon capture) (He et al., 2022; Hong, 2022). Additionally, CO₂ needs to be removed from natural gas and biogas (i.e., CO₂/CH₄ separation) (Chen, D. et al., 2023; Datta et al., 2022). For all these separations, membrane technology has attracted significant attention because of its high energy efficiency and small footprint (Chen, R. et al., 2023; Galizia et al., 2017; Han and Ho, 2021).

Commercial membranes are often based on polymers because of their low cost and excellent processability, such as cellulose acetates (Nguyen et al., 2019), Matrimid (Castro-Muñoz et al., 2018), PolarisTM (Lin et al., 2014; White et al., 2017), polydimethylsiloxane (PDMS) (Zhang and Lin, 2023), and *m*-polybenzimidazole (*m*-PBI) (Wang et al., 2022). These membranes exhibit high gas permeance, high selectivity, and good stability against aging and practical conditions.

Based on the solution-diffusion model, permeance of gas A (Q_A) can be expressed using the following equation:

$$Q_A = \frac{P_A}{I} = \frac{S_A \times D_A}{I} \tag{1}$$

where l is the selective layer thickness, and P_A , S_A , and D_A are the permeability, solubility, and diffusivity coefficient of gas A in the selective layer material, respectively. Q_A has a unit of GPU, where 1 GPU = 1×10^{-6} cm³(STP) cm⁻² s⁻¹ cmHg⁻¹ = 3.33×10^{-10} mol m⁻² s⁻¹ Pa⁻¹. Gas selectivity ($\alpha_{A/B}$) is defined as:

$$\alpha_{A/B} = \frac{Q_A}{Q_B} = \frac{P_A}{P_B} = \left(\frac{S_A}{S_B}\right) \times \left(\frac{D_A}{D_B}\right) \tag{2}$$

Solubility selectivity (S_A/S_B) is determined by their relative condensability and affinity towards polymers, and diffusivity selectivity (D_A/D_B) is controlled by their relative size difference and polymer size-sieving ability. Polymer architectures have been exhaustively manipulated to improve CO_2 separation properties, such as enhancing size sieving ability (Zhu et al., 2021; Zhu et al., 2018), imparting affinity towards CO_2 (Liu et al., 2019; Sandru et al., 2022), and achieving high free volume to attain high gas permeability (Carta et al., 2013; Luo et al., 2018; Park et al., 2007). Such approaches for CO_2 capture have been extensively reviewed (Han and Ho, 2021). Additionally, inorganic membranes with well-controlled pores and thus strong size-sieving ability have been developed for gas separations, such as graphene oxide (GO) (Wei et al., 2020; Yang et al., 2023), zeolites (Dong et al., 2021), and metal-organic frameworks (MOFs) (Drobek et al., 2015; Miao et al., 2021).

Another effective approach to increase Q_A is to decrease the selective layer thickness. As l decreases to nanoscales (such as 100 nm or less), the membrane surface becomes more important to influence gas sorption and diffusion. To this end, surface nanoengineering emerges as a new platform to improve membrane gas separation performance. Particularly, several technologies

have been developed in semiconductor industries (such as atomic layer deposition (ALD) and chemical vapor deposition (CVD)), which have been practiced at a large-scale using roll-to-roll processes and are convenient for membrane post-modification. However, very few review articles are available on this topic in the literature (Castro-Muñoz et al., 2020; Mavukkandy et al., 2020), particularly focusing on CO₂ capture.

Herein we provide a critical review of state-of-the-art surface nanoengineering technologies to develop membranes for CO₂ capture, including ALD, CVD, plasma treatment, direct fluorination, and ion/electron beam treatment, as shown in Figure 1. Ozone treatment and surface-initiated polymerization to improve gas separation properties are also briefly discussed. We highlight surface-engineered membranes using these technologies to improve CO₂ separation performance and their advantages over the state-of-the-art membranes. The pros and cons of these technology are summarized to guide future work to enable these nanotechnologies for practical membrane applications.

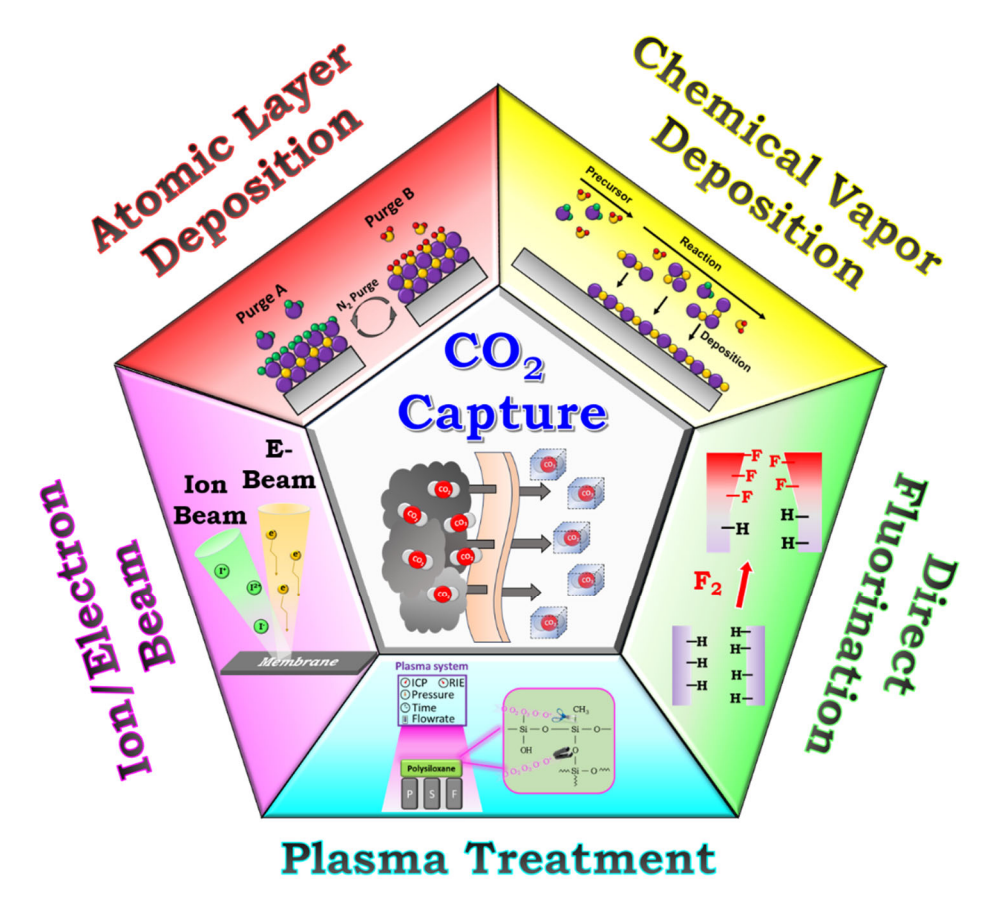


Fig. 1. Overview of five advanced surface nanoengineering technologies to develop membranes with superior CO₂ capture performance. Ozone treatment and surface-initiated polymerization are not shown here for simplicity.

2. Nanotechnologies to engineer membrane surfaces

This session describes the five nanoengineering technologies and their applications for membrane surface modification to improve CO₂ separation properties, as recorded in Table 1.

 $\textbf{Table 1.} \ Representative \ surface-nanoengineered \ membranes \ with \ enhanced \ CO_2 \ separation \ performance.$

Technologies	Membrane	Temp.	Gas permeance (GPU)				Gas selectivity			D.f.
		(°C)	H_2	CO ₂	N_2	CH ₄	H ₂ /CO ₂	CO ₂ /N ₂	CO ₂ /CH ₄	Ref.
ALD	PBI/Al ₂ O ₃ ^a	200	100	5.0	b		20			(Hu et al., 2023)
	Al_2O_3	21	909	0.18			5150			(Liu and He, 2022)
	ZIF-8	100	170	22			7.8			(Drobek et al., 2015)
	Pd	188	991	79			13			(Weber et al., 2020)
ALD-SIS	PIM-1/Al $_2$ O $_3$ ^a	35	2492	624	21.3	11.1	4.0	29	56	(Chen et al., 2021)
	$PIM\text{-}1/Al_2O_3\ ^a$	25		35	2.5	1.5		14	24	(Niu et al., 2022)
	PIM-1/TiO ₂ ^a	25		10600	710	960		15	11	
ALD-MLD	SSZ-13	200	128	31	3.6	0.30	4.1	8.6	103	(Dong et al., 2021)
CVD	Silica	500	840	0.48			1750			(Akamatsu et al., 2019)
	MOCN		202	120	1.48	1.42	1.7	81	85	(Boscher et al., 2016)
	ZIF-8		35700	11600	1590	1300	3.1	7.3	8.9	(Li et al., 2017)
	ZIF-8 HF		10600	3240		345	3.3		9.4	
Plasma	POSi	200	280	3.0			93			(Zhu et al., 2021)
		200	930	29			32			
	Pebax-TPP	35		377	11			34		(Zhao et al., 2019)
	Pebax	30		1800	42			43		(Liu et al., 2023)
	Pebax	25		2500	53			48		(Selyanchyn et al., 2020)
Direct	TR-PBOI	35	239	31	0.6	0.1	7.7	52	310	(Seong et al., 2021)
fluorination	PIM-1	35	263	179	5.6	3.3	1.5	32	54	
	FPIM-5 ^a	35	326	22.3	0.88	0.20	15	25	110	(Ma et al., 2021)
	FPIM-10 ^a	35	479	29.9	2.39	0.65	16	13	46	
	FPIM-30 a	35	540	85.3	3.24	1.29	6.5	26	66	
Ion/electron	Graphene	25	20550	3180			6.4			(Choi et al., 2018)
beam treat.	ZIF-8	23		450	71	107		6.3	4.2	(Miao et al., 2021)
Ozone	PIM-1 ^a	35	1294	443	14	11	2.9	32	41	(Ji et al., 2022)

CAP	PDMS/PEOs	35	 1210	56	 	22	 (Fu et al., 2016)
	MOF/PEOs	35	 3000	90	 	34	 (Xie et al., 2018)

Note: ^a Values are gas permeability (Barrer); ^b Data are not available.

2.1. ALD

In a typical ALD cycle, a precursor and a reactant are carried by an inert gas and successively vaporized and introduced to the membrane surface (Li et al., 2011). The precursor is first adsorbed onto the membrane surface and then reduced by the reactant, thus forming an atomic layer. With the layer-by-layer deposition, a uniform nanometer-scale layer can be formed on the membrane. Due to the self-terminating nature, the ALD process has precise control on the nanolayer composition and thickness at a molecular level (Chen et al., 2021; Ma et al., 2018).

ALD has been demonstrated to enhance gas selectivity through the following two mechanisms. First, ALD can deposit a highly selective microporous layer on the surface. For example, a porous Al₂O₃ layer of ≈39 nm was deposited on an Anodisc aluminum oxide (AAO) support after 260 cycles (Fig. 2a-d) (Liu and He, 2022). The deposited layer slightly decreased H₂ permeance from 1074 to 909 GPU and dramatically increased H₂/CO₂ selectivity from ~3 to 5150 at 21 °C (Fig. 2e), The CO₂ can be strongly adsorbed by the Al₂O₃ layer, reducing the pore size and blocking its transport. As such, after exposure to CO₂, the membrane exhibited H₂ permeance only 50% of its original value (Fig. 2f). Then during the CO₂ desorption, H₂ permeance increased and returned to its original value in 2 h. The ALD process can also be combined with other processes to fabricate a selective layer. For example, a ZnO layer was first deposited on a ceramic substrate by ALD, and then it was exposed to a ligand solution to form a ZIF-8 membrane exhibiting H₂ permeance of 170 GPU and H₂/CO₂ selectivity of 7.8 at 100 °C (Drobek et al., 2015).

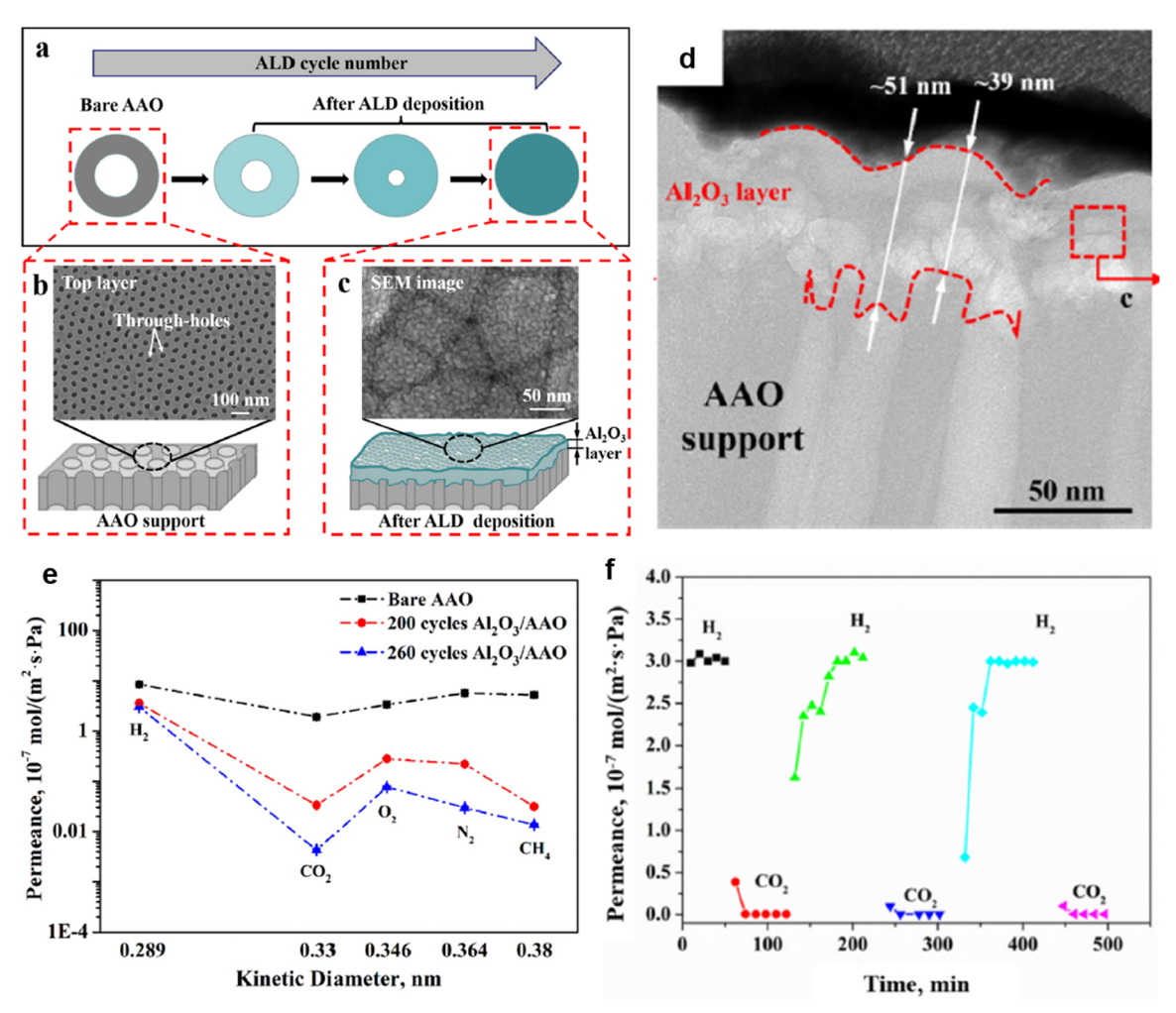


Fig. 2. (a) Schematic of Al₂O₃ ALD on an AAO support to form membranes. Diagram and surface SEM image of (b) the AAO support and (c) membrane. (d) Cross-sectional TEM image of the membrane prepared by 260 ALD cycles. (e) Pure-gas permeances at 21 °C. (f) Alternative puregas test of H₂ and CO₂ for the membrane prepared by 260 ALD cycles (Liu and He, 2022). Copyright (2022) Elsevier B.V.

Second, ALD can deposit a layer with strong affinity towards a specific gas to achieve superior separation properties. For instance, Pd layer was deposited on a porous Al₂O₃ layer by ALD, and the membrane exhibited H₂ permeance of 991 GPU and H₂/CO₂ selectivity of 13 at 188 °C due to its reactivity with H₂ (Weber et al., 2020).

In a modified ALD process, the exposure time can be increased so that the precursors can

diffuse into the membrane, which is named sequential infiltration synthesis (SIS) or vapor phase infiltration (VPI) (Hu et al., 2023). The SIS is more effective to modify the structures than its traditional counterparts, such as CVD and physical vapor deposition (PVD). Currently, SIS was mainly applied to microporous polymers because of their high diffusivity for penetrants, such as polymers of intrinsic microporosity (PIMs) (Chen et al., 2021; Niu et al., 2022) and PIM-polyimide blends (Ogieglo et al., 2020). For example, Al₂O₃ was generated on the inner pore surfaces of the PIM-1 films with a depth up to 3-5 μ m (Fig. 3a-e), which decreased the pore sizes from ~7 to < 6 Å (Fig. 3f) (Chen et al., 2021). Consequently, gas permeability decreased and CO₂/CH₄ selectivity increased by almost 3 times within 6 cycles (Fig. 3g). However, a further increase in the cycles decreased CO₂/CH₄ selectivity due to the severe blockage of the micropores for CO₂ transport. Additionally, the effect of physical aging on gas separation properties was investigated. For example, aging of 4320 h decreased CO₂ permeability by 50% from 580 to 288 Barrer but retained CO₂/CH₄ selectivity at 61 at 35 °C.

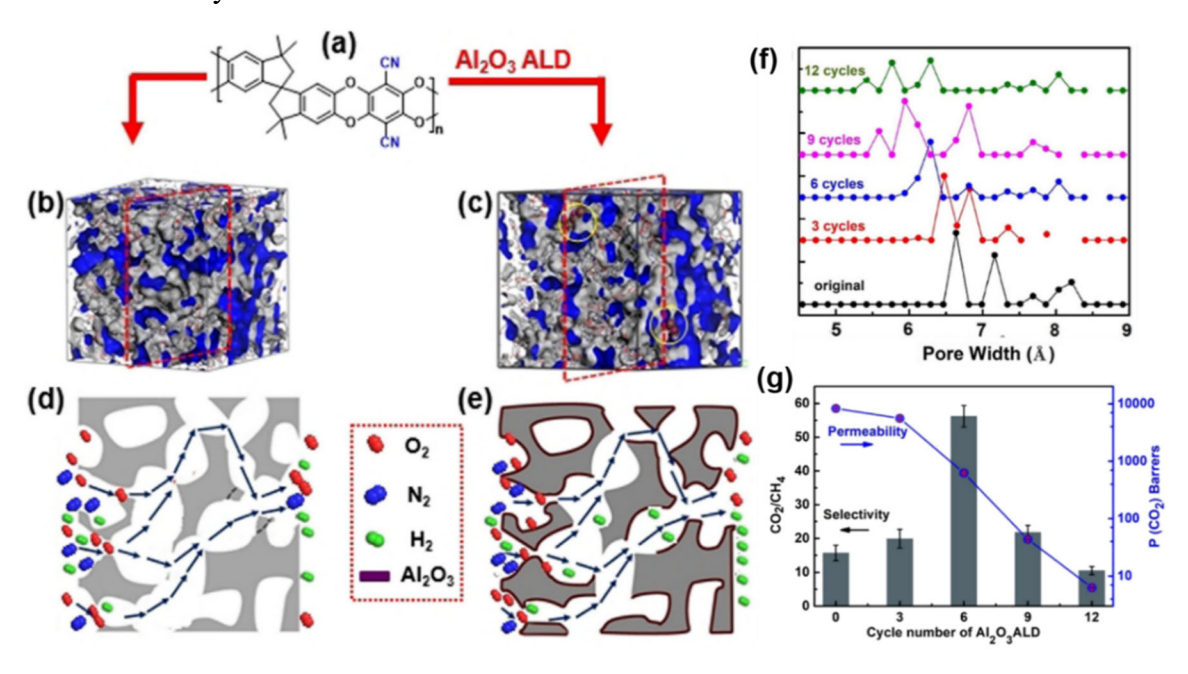


Fig. 3. (a) Chemical structure of PIM-1. 3-Dimensional pore structures of PIM-1 (b) before and (c) after the SIS. Gas transport in (d) the pristine and (e) modified PIM-1. (f) Pore size distribution as a function of SIS cycles obtained by non-local density functional theory model. (g) CO₂/CH₄ separation properties as a function of SIS cycles (Chen et al., 2021). Copyright (2021) John Wiley and Sons.

Molecular layer deposition (MLD), as an organic counterpart of ALD, can deposit a thin organic, inorganic, or hybrid layer on the membrane surface. For example, crystalline nonporous coordination polymers can also be directly prepared by MLD (Khayyami et al., 2019; Tanskanen and Karppinen, 2018); and organic ligands for MOFs can be vaporized to react with the corresponding metal sites on the surface to form a thin MOF layer (Lausund et al., 2020; Smets et al., 2023). Additionally, the as-prepared hybrid layer can be thermally treated to form porous structures with strong molecular sieving ability. For example, TiCl4 and ethylene glycol were successively vaporized and deposited on a porous SSZ-13 zeolite membrane for 30 cycles to form a dense 20-nm titanium alkoxide layer (Fig. 4a,b) (Dong et al., 2021). After calcination at 250 °C in air, the titanium alkoxide layer became porous and partially blocked surface pores of the zeolite membrane, decreasing gas permeance and increasing H₂/gas selectivity (Fig. 4c,d). Interestingly, increasing the MLD cycles from 30 to 40 decreased H₂/N₂ and H₂/CH₄ selectivity. The modified membrane also exhibited CO₂/CH₄ selectivity above 100.

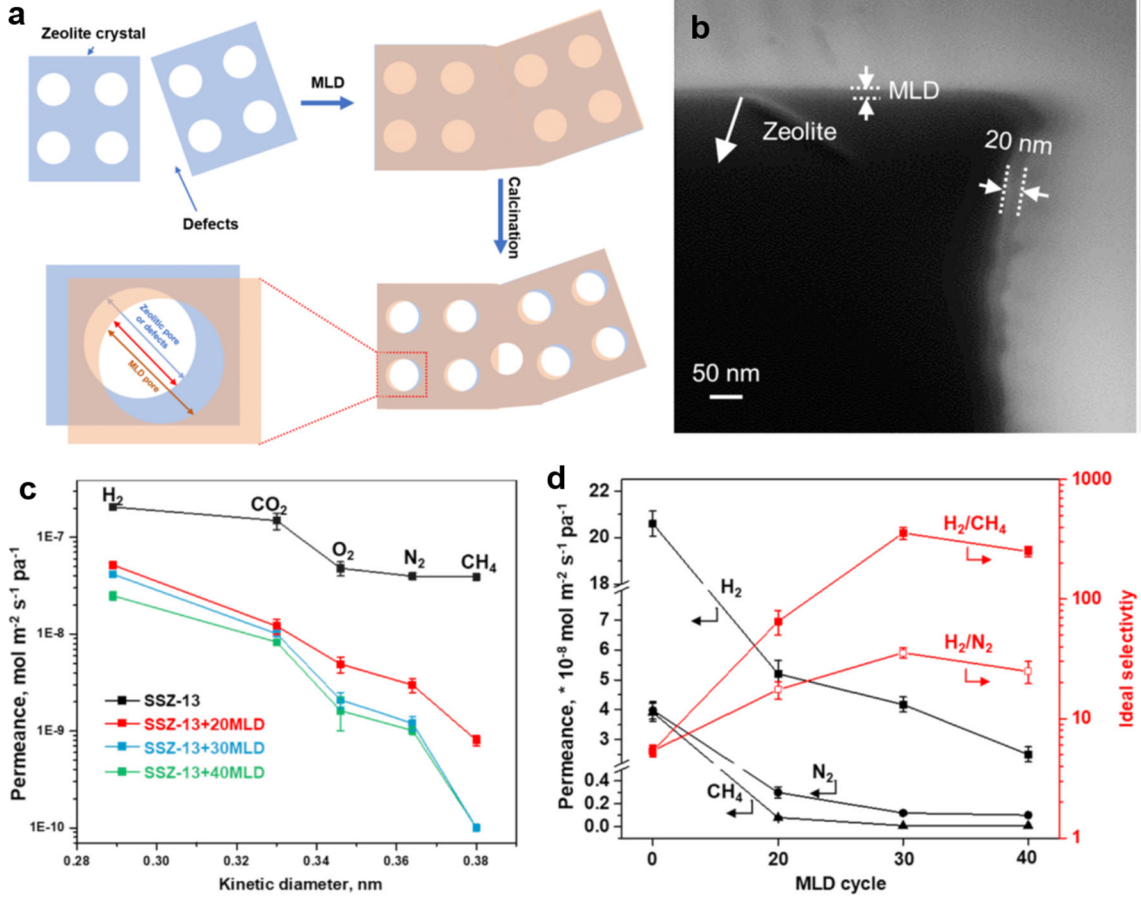


Fig. 4. (a) Schematics of MLD to eliminate defects and reduce pore sizes of SSZ-13 zeolite membranes. (b) FIB-SEM image of the membrane after 30 MLD cycles. (c) Gas permeance and (d) H₂/gas separation properties as a function of the MLD cycles at 200 °C (Dong et al., 2021). Copyright (2021) Elsevier B.V.

2.2. CVD

In a typical CVD process, volatile precursors are generated to react with the membrane or decompose on the surface or inside the porous surface, forming a thin layer, such as silica (Akamatsu et al., 2019; Anggarini et al., 2022) and graphene (Yuan et al., 2021). CVD often operates at higher temperatures than ALD processes to decompose the precursor vapors, and therefore, it requires thermally and chemically stable substrates. For example, a dimethoxydimethylsilane-derived silica membrane was fabricated using CVD and exhibited

H₂/CO₂ selectivity of 1750 and H₂ permeance of 840 GPU at 500 °C (Akamatsu et al., 2019; Khatib and Oyama, 2013).

Organic-inorganic covalent or coordinated porous frameworks could also be fabricated into a selective layer using CVD. For instance, an ultrathin metal-organic covalent network (MOCN) layer was synthesized from metalloporphyrin (zinc (II) meso-tetraphenyl porphyrin, ZnTPP) via an initiated plasma enhanced CVD (iPECVD) in four steps (Fig. 5a). Various substrates including poly[1-(trimethylsilyl)-1-propyne] (PTMSP), porous AAO, and silicon wafer, were used to demonstrate the scalability and independence of MOCN growth. ZnTPP monomer was first vaporized and introduced. Second, tert-butyl peroxide (TBPO) initiator was vaporized and dissociated into radicals by plasma. Third, the ZnTPP monomer and TBPO radicals were adsorbed onto the substrate surface. Finally, the monomer and initiator were polymerized, forming a MOCN layer with a uniform thickness, such as 200 nm on the AAO support (Fig. 5b), 55 nm on PTMSP, and 67 nm on the silicon wafer. The MOCN layer on the silicon wafer had a smooth surface with a root-mean-square roughness of only 0.6 nm (Fig. 5c), and it exhibited rigid microporous structures with a cur-off smaller than 0.4 nm due to the π - π stacking. Fig. 5d displays that the deposition of the MOCN layer on PTMSP decreased gas permeance and increased size sieving ability. For example, MOCN-1 (47 nm) exhibited a molecular cutoff between CO₂ and O₂, enabling high CO₂/gas selectivity. Increasing the MOCN thickness to 67 nm reduced the molecular cutoff to between H₂ and CO₂, leading to ultrahigh H₂/gas selectivity and decreased gas permeance (Fig. 5e).

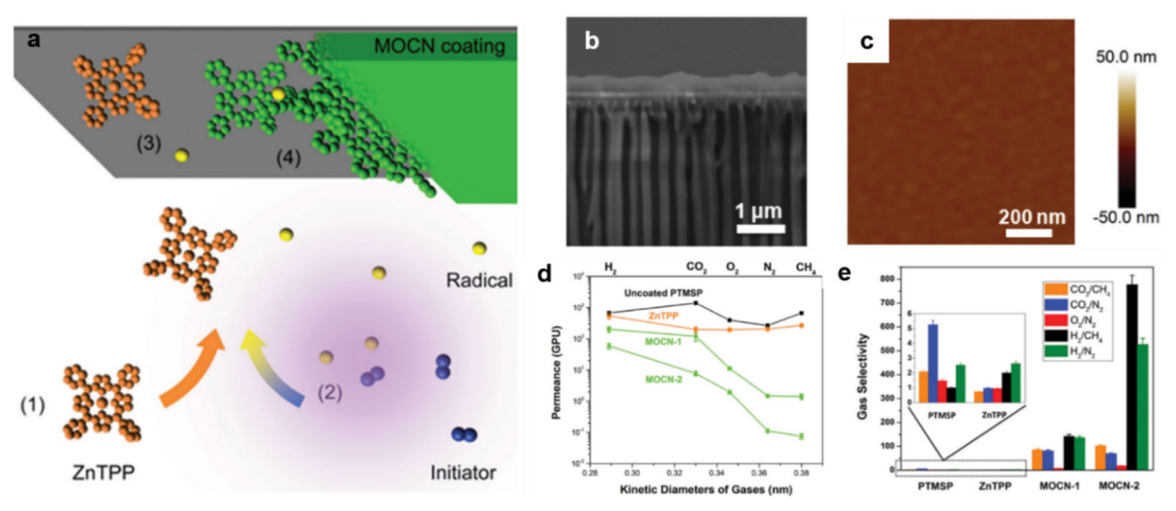


Fig. 5. (a) Schematic of the iPECVD process. (b) Cross-sectional SEM image of a 200-nm MOCN film deposited on an AAO support. (c) Atomic force microscopy (AFM) image of MOCN-coated silicon wafer with a root-mean-square roughness of 0.6 nm. (d) Gas permeance as a function of kinetic diameters. (e) Gas selectivity of PTMSP and ZnTPP- and MOCN-deposited PTMSP (Boscher et al., 2016). Copyright (2016) John Wiley and Sons.

CVD has also been used to prepare defect-free thin layers of MOFs for gas separations by optimizing processing parameters for reactant transport, heterogeneous crystallization, and fluid dynamics (Sakaida et al., 2016; Stassen et al., 2016). For example, gel-vapor deposition (GVD) was developed to form continuous ZIF-8 layers on poly(vinylidene fluoride) (PVDF) hollow fibers, including sol-gel coating and solvent-free vapor deposition. As shown in Fig. 6a,b, a solution of zinc acetate dihydrate and ethanolamine in ethanol was coated on ammoniated fibers via dipcoating. After drying, the formed gel layer was exposed to a ligand vapor (2-methylimidazole) at 150 °C to form a ZIF-8 layer as thin as 80 nm (Fig. 6c,d). Hollow fiber membranes with 280-nm ZIF-8 layer were prepared, and a module containing 340 cm² membrane exhibited H₂ permeance at 10,600 GPU, H₂/CH₄ selectivity of 30.7, and CO₂/CH₄ selectivity of 9.4.

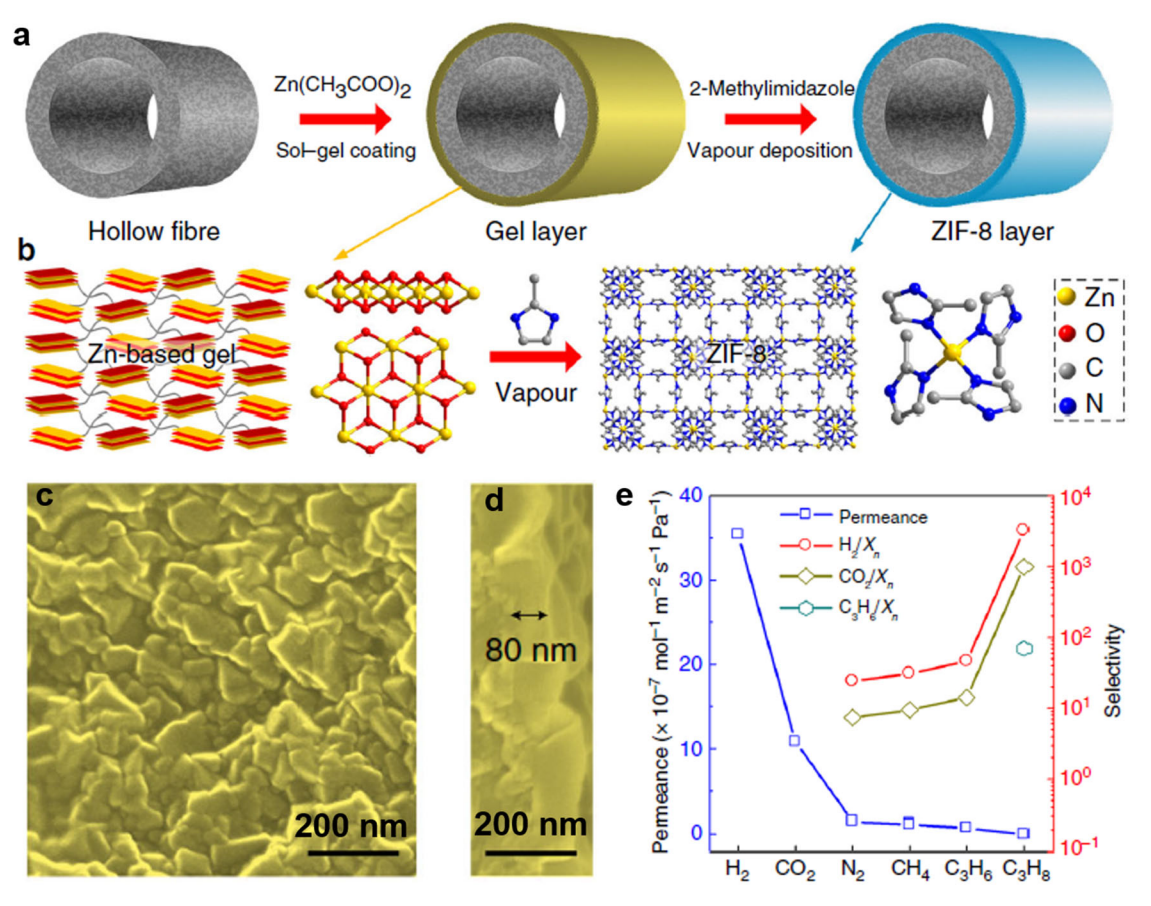


Fig. 6. (a) Schematic of ZIF-8 membrane formation via GVD. (b) Chemical structure of Zn-based gel and crystalline structure of ZIF-8. (c) Top and (d) cross-section SEM image of the ZIF-8 membrane. (e) Gas separation properties of a hollow fiber module containing 340 cm² membrane with 280-nm ZIF-8 selective layer (Li et al., 2017).

2.3. Plasma treatment

Plasma treatment can rapidly modify surfaces at ambient temperature due to highly reactive plasma species (Aoyama et al., 2022; Woo et al., 2017; Zhu et al., 2021). Generally, plasma species are generated by electron excitation and ionization of gas molecules using radio-frequency (RF) electromagnetic field (Chabert et al., 2021). The RF field can be applied capacitively between two parallel electrodes or inductively via conductive coils. In practice, these two techniques are often considered as reactive ion etching (RIE) and inductively coupled plasma (ICP), respectively. The

RIE yields low ion density with high energy and is suitable for physical etching (such as ion bombardment), while ICP renders high ion density at low energy and thus uniform and non-damaging treatment (Lee, 2018). A combination of ICP and RIE process can vertically control ion density and energy, enabling precise control of membrane surface modification.

Fig. 7a presents the schematic of an oxygen plasma treatment of PDMS-based thin-film composite (TFC) membrane in a coupled ICP-RIE system (Bui et al., 2023; Zhu et al., 2021). The oxygen was ionized by passing through an oscillating magnetic field (ICP mode) and attracted toward the membrane via an electrical bias between the atmosphere and the sample stage (RIE mode). The oxygen ions cleaved methyl (-CH₃) groups on the siloxane backbone, forming interchain Si-O-Si linkages (Fig. 7b) and porous silica-like structure (polyorganosilica or POSi) with robust molecular sieving ability. For instance, the 120-s plasma treatment increased H₂/CO₂ selectivity from 1.2 to 61 at 150 °C (Fig. 7c). Further increase in plasma treatment time to 360 s enhanced the H₂/CO₂ selectivity to 100. Additionally, the POSi membrane exhibited stable H₂/CO₂ separation performance for 340 days at simulated practical conditions, demonstrating excellent stability and promise for industrial applications.

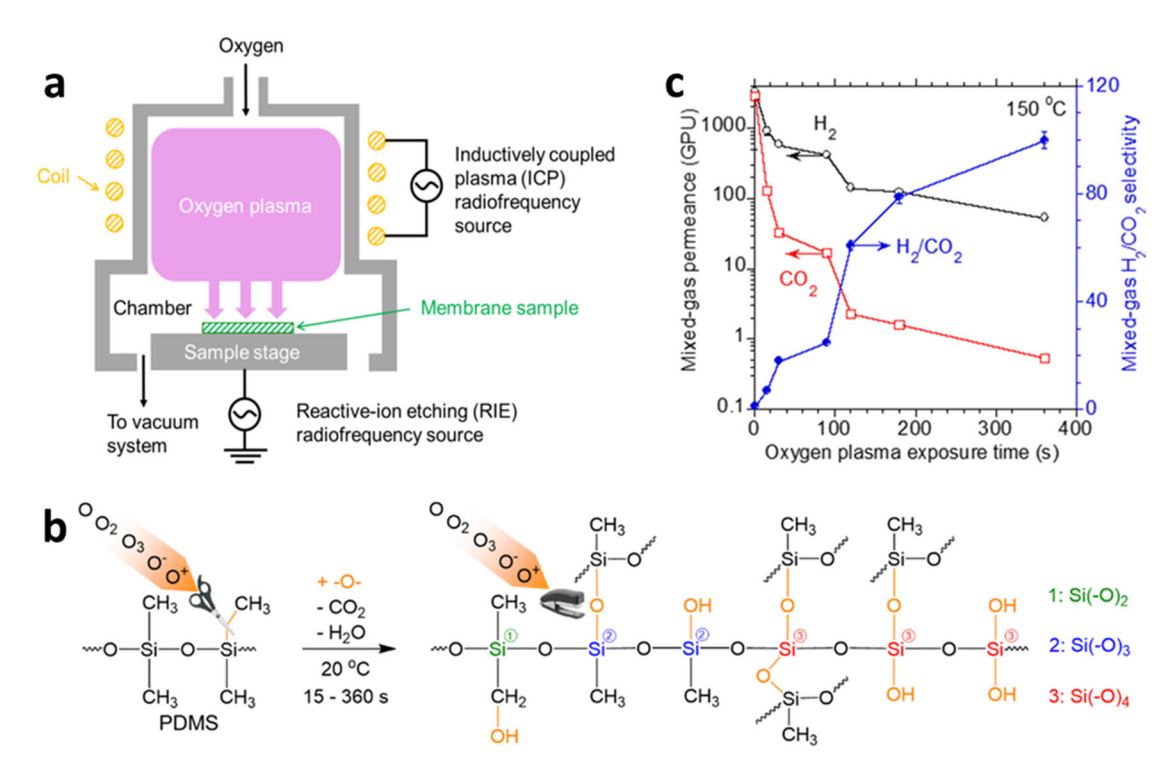


Fig. 7. (a) Schematic of oxygen plasma treatment chamber. (b) Conversion of PDMS to POSi. (c) Robust H₂/CO₂ separation performance of POSi membranes. Reproduced from (Zhu et al., 2021). Copyright (2021) American Chemical Society.

Oxygen plasma treatment can also form hydroxide groups (–OH) on the membranes and improve surface hydrophilicity. This approach can facilely tune the surface hydrophilicity of gutter layers to prepare high-performance TFC membranes (Jiang et al., 2022; Zhao et al., 2019). Fig. 8a presents the schematic of TFC membranes comprising a selective layer of Pebax 1657, a gutter layer of PDMS-poly(ethylene oxide) (PDMS-PEO), and a polyacrylonitrile (PAN) support (Liu et al., 2023). The gutter layer was treated by air plasma for less than 10 s to increase hydrophilicity (Fig. 8b) to coat ultrathin, defect-free Pebax layers (Fig. 8c), leading to CO₂/N₂ selectivity of 43 and CO₂ permeance of 1800 GPU at 30 °C.

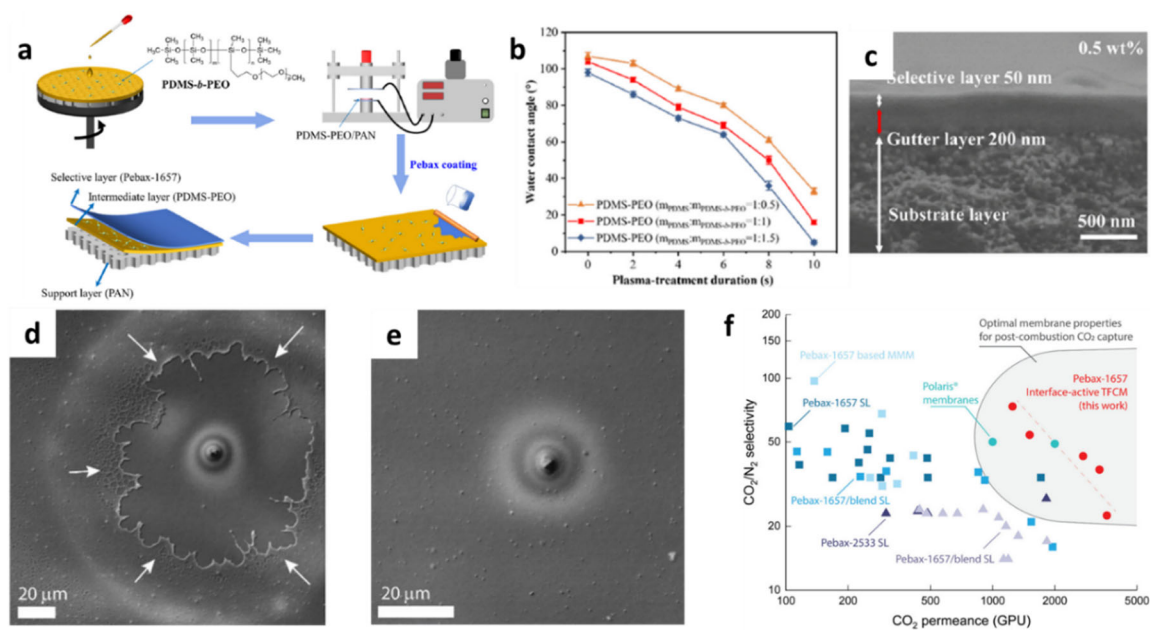


Fig. 8. (a) Fabrication of Pebax/PDMS-PEO/PAN membrane. (b) Drastic decrease in water contact angle of the PDMS-PEO gutter layer after the air plasma treatment. (c) Ultrathin Pebax layer coating on the plasma treated PDMS-PEO gutter layer. Reproduced from (Liu et al., 2023). Surface coating of Pebax on (d) the pristine and (e) oxygen-plasma treated PDMS gutter layer. (f) Superior CO₂/N₂ separation properties of Pebax/oxygen-plasma treated PDMS membrane compared with state-of-the-art membranes. Reproduced (Selyanchyn et al., 2020). Copyright (2020) American Chemical Society.

PDMS gutter layer was treated by oxygen plasma to coat defect-free Pebax selective layers (Selyanchyn et al., 2020). Fig. 8d,e compares the surface coating of Pebax on pristine PDMS and modified PDMS (by oxygen plasma for 0.7 s). The modified gutter layer led to better uniformity in the Pebax layer than the pristine PDMS. The membranes with a 20-nm Pebax layer exhibited CO₂ permeance of 2500 GPU and CO₂/N₂ selectivity of 48.

2.4. Direct fluorination

Fluorinated polymers exhibit excellent He/gas and gas/CH₄ separation properties, as well as physical and chemical stability (Okamoto et al., 2020; Wu et al., 2019). However, these polymers

are difficulty to synthesize and thus expensive. An alternative way is to directly fluorinate hydrocarbon membrane surface using fluorine to acquire advantageous characteristics of the fluorinated polymers (Belov et al., 2023; Mohr et al., 1991a; Mohr et al., 1991b). The fluorine diffuses into and reacts with the polymers with high free volume, such as PIMs (Ma et al., 2021) and thermal rearranged (TR) polymers (Seong et al., 2021). For example, the large fluorine atoms (3.65 Å) replaced the H atoms (2.89 Å) in PIM-1, decreasing pore sizes and increasing size-sieving ability (Ma et al., 2021). Specifically, 10-min fluorination changed the pore structure centered at 9.5 Å to a bimodal distribution centered at 6.1 and 8.0 Å, decreased H₂ permeability from 2772 to 479 Barrer and increased H₂/CO₂ selectivity from 0.74 to 16 at 35 °C. Similarly, PIM-1 was fluorinated using liquid perfluorodecalin and showed fluorination depths increasing linearly with the square of the fluorination time (Belov et al., 2023). The fluorination decreased permeability and increased size-sieving ability (and thus H₂/CO₂, CO₂/N₂, and CO₂/CH₄ selectivity). However, gas permeability decreased with time because of the relaxation of the free volume.

Fig. 9 displays the hierarchical pore structures in the fluorinated TR polymers using slow beam positron annihilation lifetime spectroscopy (Seong et al., 2021). Fluorination gradually decreased the τ₃ value from 2.7 ns (corresponding to a pore radius at 3.36 Å) in the bulk to 1.6 ns (2.48 Å) on the surface (with a penetrating depth of 149 nm) (Fig. 9a,b). As such, the membrane exhibited a cascaded pore size distribution (Fig. 9c). Moreover, the reduced hierarchical pores were amplified in the "throat-like" pores (Fig. 9d), increasing CO₂/CH₄ selectivity from 10 to above 100 and decreasing CO₂ permeability to 320 Barrer at 35 °C after the 300-min fluorination (Fig. 9e). Interestingly, the fluorination had a negligible effect on H₂ permeability and thus

increased H₂/CO₂ selectivity, especially at high temperatures (Fig. 9f). Additionally, membrane modules were fabricated and exhibited stable separation properties for ~9000 h, indicating their potential for industrial applications.

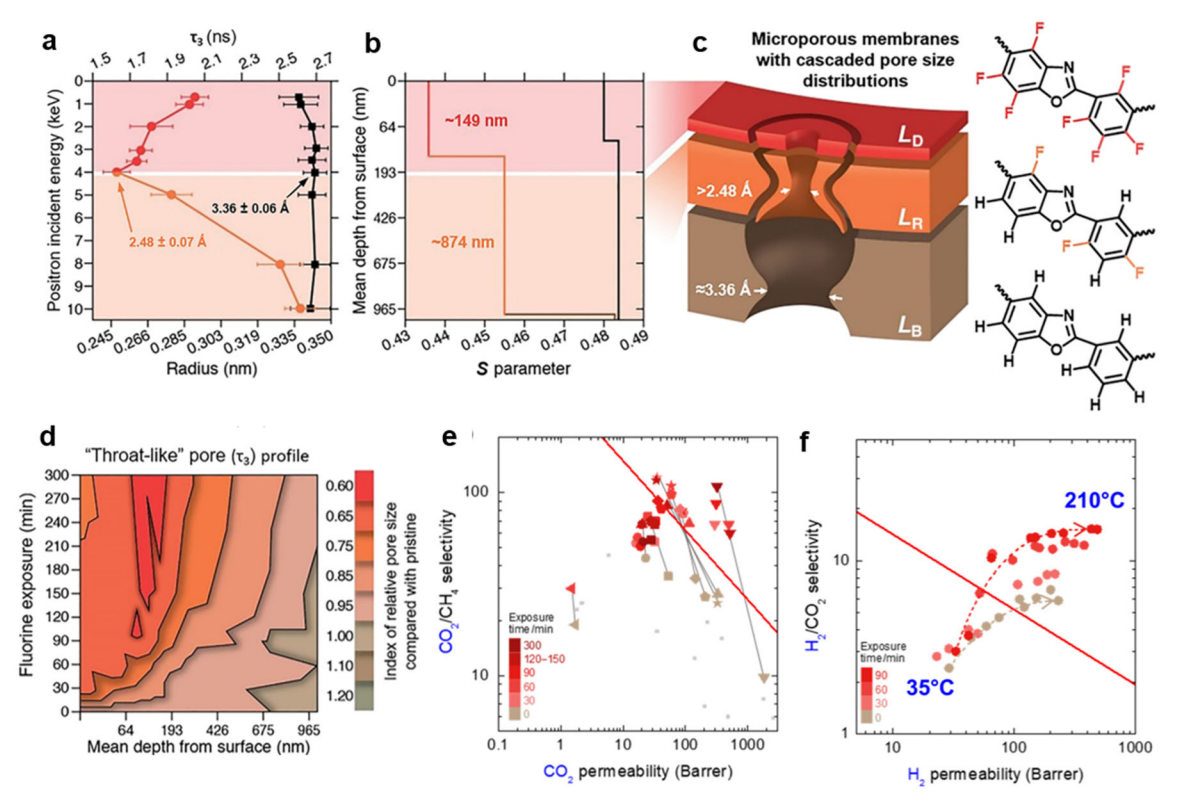


Fig. 9. Structure and separation properties of the fluorinated TR polymers. Depth profiles of (a) pore size and (b) layer thickness in fluorinated polymer (red and orange) at the near surface compared to pristine membranes (black). (c) This domain consists of a deposited layer (L_D , red, ~149 nm), and pore-regulated layer (L_R , orange, ~874 nm) on top of the bulk layer (L_B , brown). Each chemical structure indicates possible substitution positions performed at L_D , L_R , and L_B , respectively. (d) Graphical spectra built by calculating the ratio of the modified pore size to the pristine pore size and then marking each region based on the color scale. (e) CO₂/CH₄ and (f) H₂/CO₂ separation performance at elevated temperatures (Seong et al., 2021).

2.5. Ion/electron beam treatment

Ion beam treatment can effectively modify chemical structures, microstructures, and gas permeation properties of polymeric membranes (Ilconich et al., 2003). The ion beam irradiation

depends on the ion types, energy, fluence (the number of ions per unit area), and polymer precursors (Xu et al., 1995). The radiation degrades chemical bonds, releases small volatile molecules, and crosslinks polymer chains. The release of small molecules creates defects in the polymer, increasing free volume and gas permeability. Conversely, crosslinking restrains chain mobility and decreases gas permeability (Ye et al., 2019). By balancing crosslinking and degradation, ion beam irradiation can effectively improve gas separation properties. For example, H⁺ beam irradiation of Matrimid decreased CO₂ permeance and increased CO₂/N₂ and CO₂/CH₄ selectivity (Hu et al., 2007). Interestingly, increasing the ion fluence further increased CO₂/gas selectivity but barely changed CO₂ permeance.

The ion beam can form latent tracks along the ion trajectories, resulting in cylindrical pores (Apel and Fink, 2004). For example, poly(ethylene terephthalate) (PET) was etched by the 100 MeV Cl⁹⁺ ion beam to generate pores of 70 - 210 nm (Awasthi et al., 2011). The ion beam irradiation can also generate atom-scale holes on 2-dimensional (2D) materials, such as graphene (Celebi et al., 2014; Choi et al., 2018) and GO (Wei et al., 2020; Yang et al., 2023). The patterned porous graphene was fabricated via oxygen-ion beam etching with a spherical block copolymer (Choi et al., 2018). Specifically, the graphene was layered on the glass and then coated by polystyrene-block—polymethyl methacrylate (PS-*b*-PMMA) (Fig. 10a: step 1,2). After oxygen plasma and acetic acid treatment to open the PMMA phase and form a porous polymer layer (step 3), oxygen beam was used to etch and perforate the underlying graphene layer (step 4). With thermal annealing to remove the polymer residue (step 5) and laminating the graphene on a polycarbonate track-etched (PCTE) support (step 6), a composite porous graphene membrane was

prepared (step 7, and Fig. 10b). Increasing the etching time from 5 to 25 s increased the pore sizes from 18 to 30.5 nm and pore number density from 1.25×10^{10} to 2.1×10^{10} cm⁻² (Fig. 10c). Nevertheless, the membrane exhibited H₂/CO₂ selectivity of <10 because of the large pores and weak size-sieving ability.

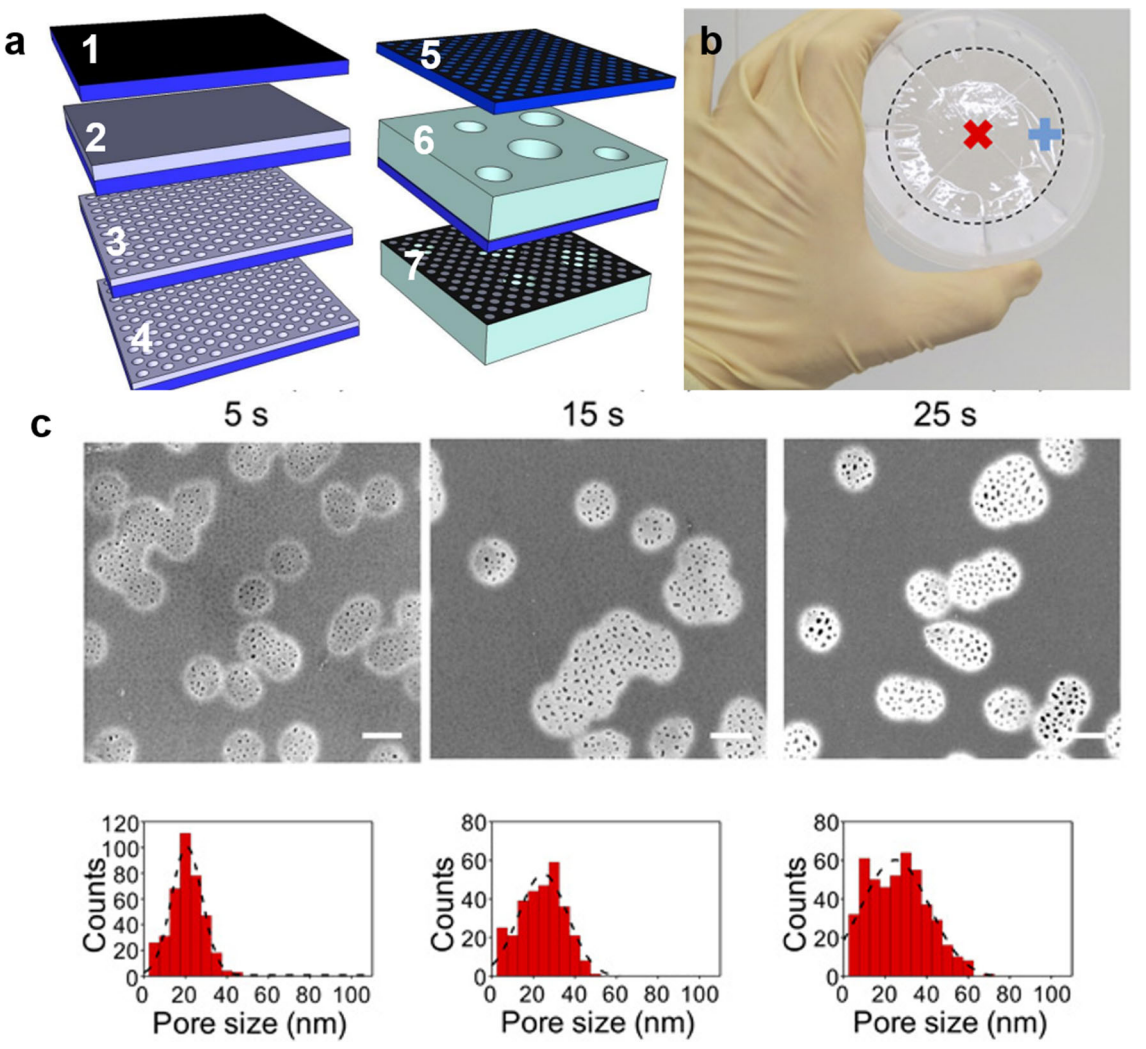


Fig. 10. (a) Schematic of the 7-step manufacturing process of patterned porous graphene and its composite membrane. (b) Photo of a PCTE-supported porous graphene membrane. (c) SEM images and pore size distributions of PCTE-supported porous graphene membranes with various oxygen beam treatment times (Choi et al., 2018).

Electron beam (e-beam) irradiation can also modify chemical properties and then tune the

affinity towards gas molecules (Tu et al., 2021). For instance, a ZIF-8 membrane was treated with electron doses between 0.017 and 10 mC cm⁻² (Fig. 11a) (Miao et al., 2021). The 1-min e-beam irradiation decreased CO₂ permeance by 20% from 570 to 450 GPU (Fig. 11b) and increased CO₂/N₂ selectivity from 1.6 to 6.3 and CO₂/CH₄ selectivity from 1.3 to 4.2. However, increasing the irradiation time to 5 mins or longer decreased CO₂ permeance and selectivity simultaneously. At the beginning, the e-beam irradiation broke the Zn/imidazolate ligand coordination and generated –NH groups, as confirmed by the X-ray photoelectron spectra (XPS) spectra (Fig. 11c,d). The –NH groups exhibited high affinity towards CO₂ and enhanced CO₂ sorption in the membrane. On the other hand, the increased irradiation dose cross-linked imidazolate ligands, blocking the pores. The Glazing-incident small angle X-ray Scattering (GISAXS) patterns confirmed that increasing the irradiation time weakened the intensity of the crystalline peaks, indicating the amorphization or collapsed pore structures in ZIF-8 (Fig. 11f).

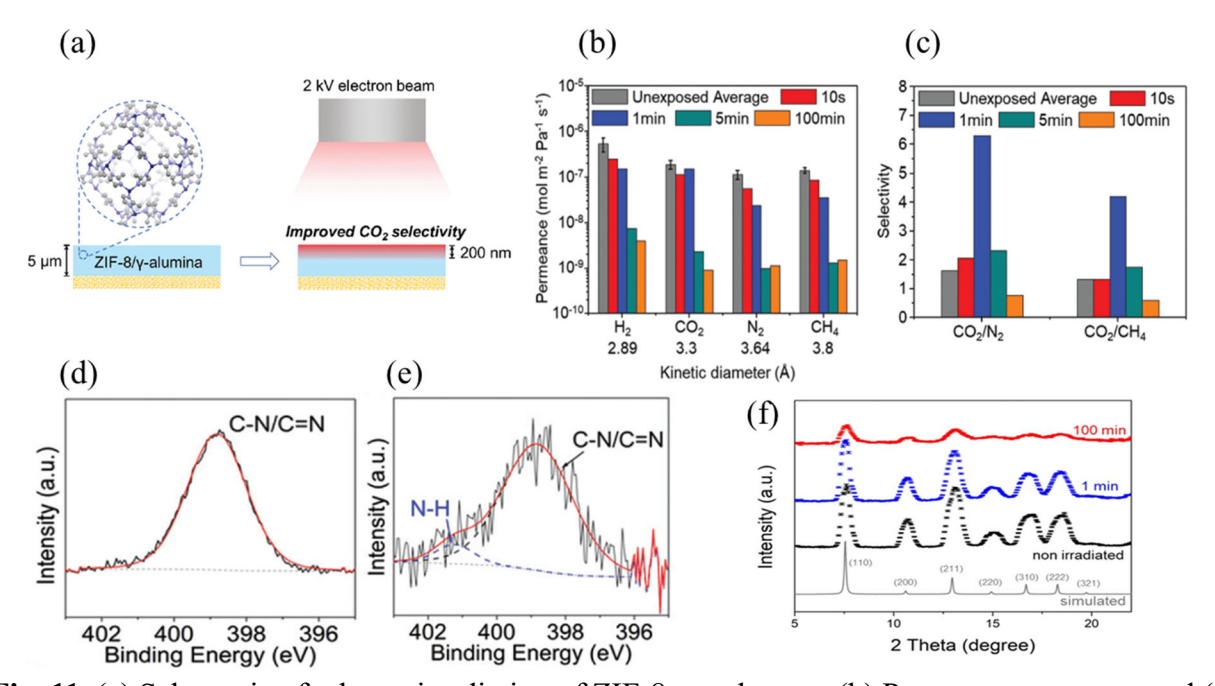


Fig. 11. (a) Schematic of e-beam irradiation of ZIF-8 membranes. (b) Pure-gas permeance and (c)

CO₂/N₂ and CO₂/CH₄ selectivity before and after the e-beam irradiation. N 1s XPS spectra (d) before and (e) after 54-min e-beam exposure. (f) GISAXS patterns of non-irradiated and e-beam irradiated films (Miao et al., 2021). Copyright (2021) Royal Society of Chemistry.

2.6. Other technologies for surface modification

Many other technologies have been adopted to modify membrane surface to improve high performance. Without intending to exhaustively review these technologies, we briefly discuss two of them, including ozone treatment and surface-initiated polymerization such as continuous assembly of polymers (CAP).

UV and UV-ozone can modify the surface chemistry, especially for PDMS membranes (Fu et al., 2010; Lai et al., 2012; Ouyang et al., 2000). Moreover, ozone treatment can even tune pore structures of PIM-1 (Ji et al., 2022). Specifically, the ozone oxidized benzene rings on the PIM-1 polymer chains and induced functional groups, such as COOH and C=O groups. The 3D structure simulation showed that the oxidation changed the multi-pore structures of pristine PIM-1 (5.3, 7.6 and 12 Å) to only one ultramicropore at 3.8 Å, thus enhancing the molecular sieving ability. For example, 60-s ozone treatment decreased CO₂ permeability from 4868 to 443 Barrer at 35 °C, leading to an increase of CO₂/N₂ selectivity from 19 to 32 and CO₂/CH₄ selectivity from 15 to 41. However, increasing pressure decreased CO₂/CH₄ selectivity because of CO₂-induced plasticization.

CAP technology allows an in situ growth of a thin selective layer (<30 nm) exhibiting superior CO₂ separation properties (Fu et al., 2016; Xie et al., 2018). Specifically, a gutter layer was first prepared on a porous substrate, and then its surface was functionalized with a bromide initiator for

atom transfer radical polymerization (ATRP). Second, PEO-based macro-cross-linkers were introduced and polymerized on the initiator sites, forming a thin defect-free selective layer. For example, an ultra-thin PEO-based layer (~30 nm) was grown on a MOF gutter layer, achieving CO₂ permeance of 3000 GPU and CO₂/N₂ selectivity of 34 at 35 °C (Xie et al., 2018). However, a 45-day aging of the membrane decreased CO₂ permeance by 30% and CO₂/N₂ selectivity by 40%.

3. Superior CO₂ capture performance in surface-engineered membranes

Fig. 12 demonstrates the advantages of surface-nanoengineered membranes for H₂/CO₂, CO₂/N₂, and CO₂/CH₄ Separation. For instance, compared to PBI, one of leading materials for H₂/CO₂ separation (Hu et al., 2021), the surface-modified materials exhibit high H₂ permeance because of their porous structures, and most of them (particularly ALD- and CVD-treated ones) exhibited H₂/CO₂ separation properties surpassing the upper bound at 35 °C.

The surface-modified membranes also showed attractive CO₂/N₂ separation properties near the upper bound (Fig. 12b). Particularly, the Pebax-based TFC membranes containing a plasmatreated gutter layer exhibited CO₂/N₂ separation properties superior to the leading amorphous PEO-based membrane (Zhang et al., 2022). The surface-fluorinated membranes (such as PIM-1) exhibited CO₂/CH₄ selectivity as high as 300 (Fig. 12c), surpassing the upper bound and superior to the leading Matrimid hollow fiber membranes (Dong et al., 2010; Karvan et al., 2013).

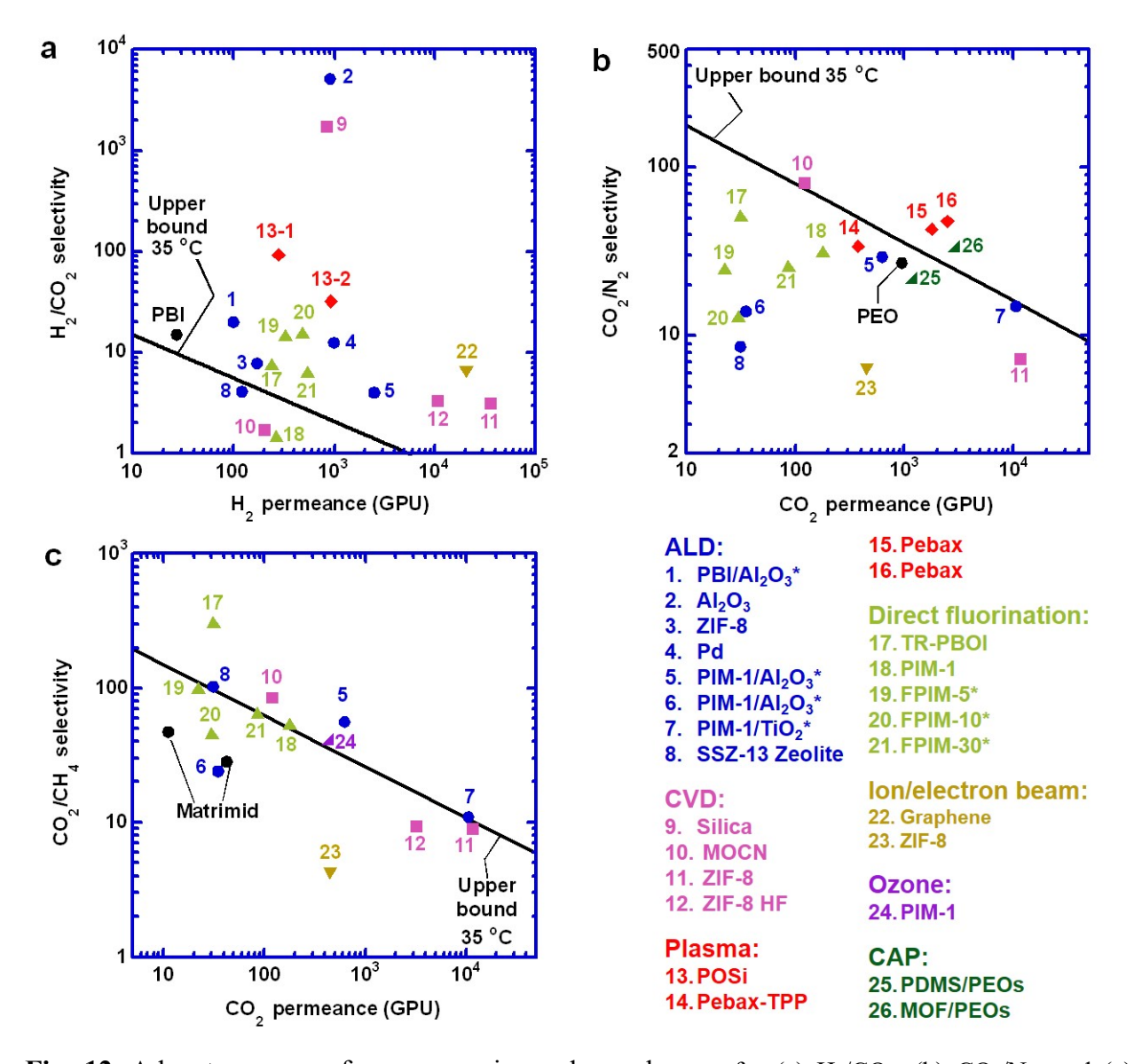


Fig. 12. Advantageous surface-nanoengineered membranes for (a) H_2/CO_2 , (b) CO_2/N_2 , and (c) CO_2/CH_4 separations benchmarked with the upper bounds at 35 °C. The upper bounds and materials marked with the * symbol are based on 1 μ m-thick layers. More details are shown in Table 1. Data of PBI, PEO, and Matrimid are from (Dong et al., 2010; Hu et al., 2021; Karvan et al., 2013; Zhang et al., 2022).

4. Conclusions

We thoroughly review state-of-the-art nanotechnologies to modify membrane surface to improve CO₂ capture performance, including ALD, CVD, plasma treatment, direct fluorination,

and ion/electron beam treatment. Because of the thin nature of the selective layer, the modification of surface chemistry and structure at nanoscales can effectively exert significant impact on gas sorption and diffusion behavior. Their pros and cons are summarized below.

- 1) Both ALD and CVD processes can deposit an extremely thin layer on the surface with controlled thickness, structure and chemistry, which can be used to finetune membrane surface chemistry and pore sizes and thus gas separation properties. Both technologies hold great potential to improve membrane separation performance at a large scale, though the cost of operation needs to be thoroughly investigated. Additionally, the porous supports need to withstand high temperature and highly active conditions, especially for CVD.
- 2) Oxygen plasma treatment provides a fast and facile way to impart hydrophilicity to polysiloxanes or form a thin silica layer on polysiloxanes with superior H₂/CO₂ separation properties, performance. The process has the potential to be adapted for large-scale membrane modification. However, roll-to-roll plasma treatment at low pressures need to be demonstrated to achieve the controllability and uniformity of the silica layer.
- 3) Direct fluorination effectively imparts fluorine groups on the membrane surface, achieving unique properties of fluorinated polymers, such as hydrocarbon-phobicity, chemical stability, and most importantly, superior gas separation properties. However, the fluorination degree cannot be easily controlled, and gas permeance might decrease with time.
- 4) The ion/electron beam irradiation can simultaneously increase free volume by degradation and chain rigidity by cross-linking. The parameters can be optimized to improve gas transport properties. However, it is challenging to precisely control surface chemistry and structures.

5) UV treatment and surface-initiated polymerization can effectively modify membrane surface and improve gas separation properties. Both technologies might have the potential for large-scale manufacturing of membranes, which, however, are yet to be demonstrated.

We expect that the surface-engineering nanotechnologies have the potential to be integrated into the existing membrane manufacturing processes to produce high-performance carbon-capture membranes in an economically viable way. The additional costs derived from the technologies need to be evaluated and justified for the improved membrane properties and system performance. As the surface nanoengineering technologies are gaining more uses at large scale in various industries, their marriage with the membrane industry will become more practical, considering their capabilities of significantly enhancing CO₂ capture performance.

Acknowledgements

This work was funded by the U.S. Department of Energy (DOE) National Energy Technology Laboratory (NETL # DE-FE0032209) and National Science Foundation (NSF # 2044623).

References

- Akamatsu, K., Suzuki, M., Nakao, A., Nakao, S.-i., 2019. Development of hydrogen-selective dimethoxydimethylsilane-derived silica membranes with thin active separation layer by chemical vapor deposition. J. Membr. Sci. 580, 268-274.
- Anggarini, U., Nagasawa, H., Kanezashi, M., Tsuru, T., 2022. Structural two-phase evolution of aminosilica-based silver-coordinated membranes for increased hydrogen separation. J. Membr. Sci. 642, 119962.
- Aoyama, S., Nagasawa, H., Kanezashi, M., Tsuru, T., 2022. Nanogradient Hydrophilic/hydrophobic organosilica membranes developed by atmospheric-pressure plasma to enhance pervaporation performance. ACS Nano 16(7), 10302-10313.

- Apel, P.Y., Fink, D., 2004. Ion-track etching, in: Fink, D. (Ed.) Transport processes in ion-irradiated polymers. Springer Berlin, Heidelbergzh, pp. 147-202.
- Awasthi, K., Stamm, M., Abetz, V., Vijay, Y., 2011. Large area Cl⁹⁺ irradiated PET membranes for hydrogen separation. Int. J. Hydrog. Energy 36(15), 9374-9381.
- Belov, N.A., Alentiev, A.Y., Nikiforov, R.Y., Chirkov, S.V., Bezgin, D.A., Syrtsova, D.A., Ryzhikh, V.E., Ponomarev, I., 2023. Gas separation properties of PIM-1 films treated by elemental fluorine in liquid perfluorodecalin. Polymer 280, 126033.
- Boscher, N.D., Wang, M., Perrotta, A., Heinze, K., Creatore, M., Gleason, K.K., 2016. Metalorganic covalent network chemical vapor deposition for gas separation. Adv. Mater. 28(34), 7479-7485.
- Bui, V.T., Satti, V.R., Haddad, E., Hu, L., Deng, E., Zhu, L., Lee, W.-I., Yin, Y., Kisslinger, K., Zhang, Y., Bui, T.T., Rajapakse, B.M., Velarde, L., Nam, C.-Y., Lin, H., 2023. Ultrathin polyorganosilica membranes synthesized by oxygen-plasma treatment of polysiloxanes for H₂/CO₂ separation. J. Membr. Sci. 688, 122099.
- Carta, M., Malpass-Evans, R., Croad, M., Rogan, Y., Jansen, J.C., Bernardo, P., Bazzarelli, F., McKeown, N.B., 2013. An efficient polymer molecular sieve for membrane gas separations. Science 339(6117), 303-307.
- Castro-Muñoz, R., Agrawal, K.V., Coronas, J., 2020. Ultrathin permselective membranes: The latent way for efficient gas separation. RSC Adv. 10(21), 12653-12670.
- Castro-Muñoz, R., Martin-Gil, V., Ahmad, M.Z., Fíla, V., 2018. Matrimid® 5218 in preparation of membranes for gas separation: Current state-of-the-art. Chem. Eng. Commun. 205(2), 161-196.
- Celebi, K., Buchheim, J., Wyss, R.M., Droudian, A., Gasser, P., Shorubalko, I., Kye, J.-I., Lee, C., Park, H.G., 2014. Ultimate permeation across atomically thin porous graphene. Science 344(6181), 289-292.
- Chabert, P., Tsankov, T.V., Czarnetzki, U., 2021. Foundations of capacitive and inductive radio-frequency discharges. Plasma Sci. Technol. 30(2), 024001.
- Chen, D., Wang, K., Yuan, Z., Lin, Z., Zhang, M., Li, Y., Tang, J., Liang, Z., Li, Y., Chen, L., 2023. Boosting Membranes for CO₂ Capture toward Industrial Decarbonization. Carbon Capture Sci. Tech., 100117.
- Chen, R., Chai, M., Hou, J., 2023. Metal-organic framework-based mixed matrix membranes for gas separation: recent advances and opportunities. Carbon Capture Sci. Tech., 100130.
- Chen, X., Wu, L., Yang, H., Qin, Y., Ma, X., Li, N., 2021. Tailoring the microporosity of polymers of intrinsic microporosity for advanced gas separation by atomic layer deposition. Angew. Chem. Int. Ed. 60(33), 17875-17880.
- Choi, K., Droudian, A., Wyss, R.M., Schlichting, K.-P., Park, H.G., 2018. Multifunctional wafer-scale graphene membranes for fast ultrafiltration and high permeation gas separation. Sci. Adv. 4(11), eaau0476.
- Datta, S.J., Mayoral, A., Murthy Srivatsa Bettahalli, N., Bhatt, P.M., Karunakaran, M., Carja, I.D., Fan, D., Graziane M. Mileo, P., Semino, R., Maurin, G., Terasaki, O., Eddaoudi, M., 2022. Rational design of mixed-matrix metal-organic framework membranes for molecular

- separations. Science 376(6597), 1080-1087.
- Dong, G., Li, H., Chen, V., 2010. Factors affect defect-free Matrimid® hollow fiber gas separation performance in natural gas purification. J. Membr. Sci. 353(1-2), 17-27.
- Dong, Q., Jiang, J., Li, S., Yu, M., 2021. Molecular layer deposition (MLD) modified SSZ-13 membrane for greatly enhanced H₂ separation. J. Membr. Sci. 622, 119040.
- Drobek, M., Bechelany, M., Vallicari, C., Abou Chaaya, A., Charmette, C., Salvador-Levehang, C., Miele, P., Julbe, A., 2015. An innovative approach for the preparation of confined ZIF-8 membranes by conversion of ZnO ALD layers. J. Membr. Sci. 475, 39-46.
- Fu, Q., Kim, J., Gurr, P.A., Scofield, J.M., Kentish, S.E., Qiao, G.G., 2016. A novel cross-linked nano-coating for carbon dioxide capture. Energy Environ. Sci. 9(2), 434-440.
- Fu, Y.-J., Qui, H.-z., Liao, K.-S., Lue, S.J., Hu, C.-C., Lee, K.-R., Lai, J.-Y., 2010. Effect of UV-ozone treatment on poly(dimethylsiloxane) membranes: surface characterization and gas separation performance. Langmuir 26(6), 4392-4399.
- Galizia, M., Chi, W.S., Smith, Z.P., Merkel, T.C., Baker, R.W., Freeman, B.D., 2017. 50th Anniversary perspective: Polymers and mixed matrix membranes for gas and vapor separation: A review and prospective opportunities. Macromolecules 50(20), 7809-7843.
- Han, Y., Ho, W.S., 2021. Polymeric membranes for CO₂ separation and capture. J. Membr. Sci. 628, 119244.
- He, X., Chen, D., Liang, Z., Yang, F., 2022. Insight and comparison of energy-efficient membrane processes for CO₂ capture from flue gases in power plant and energy-intensive industry. Carbon Capture Sci. Tech. 2, 100020.
- Hong, W.Y., 2022. A techno-economic review on carbon capture, utilisation and storage systems for achieving a net-zero CO₂ emissions future. Carbon Capture Sci. Tech. 3, 100044.
- Hu, L., Bui, V.T., Huang, L., Singh, R.P., Lin, H., 2021. Facilely Cross-linking Polybenzimidazole with Polycarboxylic Acids to Improve H₂/CO₂ Separation Performance. ACS Appl. Mater. Interfaces 13(10), 12521-12530.
- Hu, L., Lee, W.-I., Subramanian, A., Deng, E., Kisslinger, K., Fan, S., Bui, V.T., Ding, Y., Nam, C.-Y., Lin, H., 2023. Few-Cycle Atomic Layer Deposition to Nanoengineer Polybenzimidazole for H₂/CO₂ Separation. Submitted.
- Hu, L., Xu, X., Coleman, M.R., 2007. Impact of H⁺ ion beam irradiation on Matrimid®. II. Evolution in gas transport properties. J. Appl. Polym. Sci. 103(3), 1670-1680.
- Ilconich, J.B., Xu, X., Coleman, M., Simpson, P., 2003. Impact of ion beam irradiation on microstructure and gas permeance of polysulfone asymmetric membranes. J. Membr. Sci. 214(1), 143-156.
- Ji, W., Geng, H., Chen, Z., Dong, H., Matsuyama, H., Wang, H., Wang, H., Li, J., Shi, W., Ma, X., 2022. Facile tailoring molecular sieving effect of PIM-1 by in-situ O₃ treatment for high performance hydrogen separation. J. Membr. Sci. 662, 120971.
- Jiang, X., Goh, K., Wang, R., 2022. Air plasma assisted spray coating of Pebax-1657 thin-film composite membranes for post-combustion CO₂ capture. J. Membr. Sci. 658, 120741.
- Karvan, O., Johnson, J.R., Williams, P.J., Koros, W.J., 2013. A pilot-scale system for carbon molecular sieve hollow fiber membrane manufacturing. Chem. Eng. Technol. 36(1), 53-61.

- Khatib, S.J., Oyama, S.T., 2013. Silica membranes for hydrogen separation prepared by chemical vapor deposition (CVD). Sep. Purif. Technol. 111, 20-42.
- Khayyami, A., Philip, A., Karppinen, M., 2019. Atomic/Molecular Layer Deposited Iron-Azobenzene Framework Thin Films for Stimuli-Induced Gas Molecule Capture/Release. Angew. Chem. Int. Ed. 58(38), 13400-13404.
- Lai, C.-L., Fu, Y.-J., Chen, J.-T., An, Q.-F., Liao, K.-S., Fang, S.-C., Hu, C.-C., Lee, K.-R., 2012. Pervaporation separation of ethanol/water mixture by UV/O₃-modified PDMS membranes. Sep. Purif. Technol. 100, 15-21.
- Lausund, K.B., Olsen, M.S., Hansen, P.-A., Valen, H., Nilsen, O., 2020. MOF thin films with biaromatic linkers grown by molecular layer deposition. J. Mater. Chem. A 8(5), 2539-2548.
- Lee, H.-C., 2018. Review of inductively coupled plasmas: Nano-applications and bistable hysteresis physics. Appl. Phys. Rev. 5(1), 011108.
- Li, F., Li, L., Liao, X., Wang, Y., 2011. Precise pore size tuning and surface modifications of polymeric membranes using the atomic layer deposition technique. J. Membr. Sci. 385(1-2), 1-9.
- Li, W., Su, P., Li, Z., Xu, Z., Wang, F., Ou, H., Zhang, J., Zhang, G., Zeng, E., 2017. Ultrathin metal—organic framework membrane production by gel-vapour deposition. Nat. Commun. 8(1), 406.
- Lin, H., He, Z., Sun, Z., Vu, J., Ng, A., Mohammed, M., Kniep, J., Merkel, T.C., Wu, T., Lambrecht, R.C., 2014. CO₂-selective membranes for hydrogen production and CO₂ capture—Part I: Membrane development. J. Membr. Sci. 457, 149-161.
- Liu, J., Pan, Y., Xu, J., Wang, Z., Zhu, H., Liu, G., Zhong, J., Jin, W., 2023. Introducing amphipathic copolymer into intermediate layer to fabricate ultra-thin Pebax composite membrane for efficient CO₂ capture. J. Membr. Sci. 667, 121183.
- Liu, J., Zhang, S., Jiang, D., Doherty, C.M., Hill, A.J., Cheng, C., Park, H., Lin, H., 2019. Highly polar but amorphous polymers with robust membrane CO₂/N₂ separation performance. Joule 3(8), 1881-1894.
- Liu, X., He, D., 2022. Atomic layer deposited aluminium oxide membranes for selective hydrogen separation through molecular sieving. J. Membr. Sci. 662, 121011.
- Luo, S., Zhang, Q., Zhu, L., Lin, H., Kazanowska, B.A., Doherty, C.M., Hill, A.J., Gao, P., Guo, R., 2018. Highly Selective and Permeable Microporous Polymer Membranes for Hydrogen Purification and CO₂ Removal from Natural Gas. Chem. Mater. 30(15), 5322-5332.
- Ma, X., Kumar, P., Mittal, N., Khlyustova, A., Daoutidis, P., Mkhoyan, K.A., Tsapatsis, M., 2018. Zeolitic imidazolate framework membranes made by ligand-induced permselectivation. Science 361(6406), 1008-1011.
- Ma, X., Li, K., Zhu, Z., Dong, H., Lv, J., Wang, Y., Pinnau, I., Li, J., Chen, B., Han, Y., 2021. High-performance polymer molecular sieve membranes prepared by direct fluorination for efficient helium enrichment. J. Mater. Chem. A 9(34), 18313-18322.
- Mavukkandy, M.O., McBride, S.A., Warsinger, D.M., Dizge, N., Hasan, S.W., Arafat, H.A., 2020. Thin film deposition techniques for polymeric membranes—A review. J. Membr. Sci. 610, 118258.

- Miao, Y., Lee, D.T., de Mello, M.D., Abdel-Rahman, M.K., Corkery, P., Boscoboinik, J.A., Fairbrother, D.H., Tsapatsis, M., 2021. Electron beam induced modification of ZIF-8 membrane permeation properties. Chem. Comm. 57(43), 5250-5253.
- Mohr, J., Paul, D., Mlsna, T., Lagow, R., 1991a. Surface fluorination of composite membranes. Part I. Transport properties. J. Membr. Sci. 55(1-2), 131-148.
- Mohr, J., Paul, D., Pinnau, I., Koros, W., 1991b. Surface fluorination of polysulfone asymmetric membranes and films. J. Membr. Sci. 56(1), 77-98.
- Nguyen, H., Wang, M., Hsiao, M., Nagai, K., Ding, Y., Lin, H., 2019. Suppression of crystallization in thin films of cellulose diacetate and its effect on CO₂/CH₄ separation properties. J. Membr. Sci. 586, 7-14.
- Niu, X., Dong, G., Li, D., Zhang, Y., Zhang, Y., 2022. Atomic layer deposition modified PIM-1 membranes for improved CO₂ separation: A comparative study on the microstructure-performance relationships. J. Membr. Sci. 664, 121103.
- Ogieglo, W., Puspasari, T., Hota, M.K., Wehbe, N., Alshareef, H.N., Pinnau, I., 2020. Nanohybrid thin-film composite carbon molecular sieve membranes. Mater. Today Nano 9, 100065.
- Okamoto, Y., Chiang, H.C., Fang, M.F., Galizia, M., Merkel, T., Yavari, M., Nguyen, H., Lin, H., 2020. Perfluorodioxolane Polymers for Gas Separation Membrane Applications. Membranes 10(12), 394.
- Ouyang, M., Muisener, R., Boulares, A., Koberstein, J., 2000. UV–ozone induced growth of a SiOx surface layer on a cross-linked polysiloxane film: characterization and gas separation properties. J. Membr. Sci. 177(1-2), 177-187.
- Park, H., Jung, C., Lee, Y., Hill, A.J., Pas, S.J., Mudie, S.T., Van Wagner, E., Freeman, B.D., Cookson, D.J., 2007. Polymers with cavities tuned for fast selective transport of small molecules and ions. Science 318(5848), 254-258.
- Sakaida, S., Otsubo, K., Sakata, O., Song, C., Fujiwara, A., Takata, M., Kitagawa, H., 2016. Crystalline coordination framework endowed with dynamic gate-opening behaviour by being downsized to a thin film. Nat. Chem. 8(4), 377-383.
- Sandru, M., Sandru, E.M., Ingram, W.F., Deng, J., Stenstad, P.M., Deng, L., Spontak, R.J., 2022. An integrated materials approach to ultrapermeable and ultraselective CO₂ polymer membranes. Science 376(6588), 90-94.
- Selyanchyn, O., Selyanchyn, R., Fujikawa, S., 2020. Critical role of the molecular interface in double-layered Pebax-1657/PDMS nanomembranes for highly efficient CO₂/N₂ gas separation. ACS Appl. Mater. Interfaces 12(29), 33196-33209.
- Seong, J.G., Lee, W.H., Lee, J., Lee, S.Y., Do, Y.S., Bae, J.Y., Moon, S.J., Park, C.H., Jo, H.J., Kim, J.S., 2021. Microporous polymers with cascaded cavities for controlled transport of small gas molecules. Sci. Adv. 7(40), eabi9062.
- Smets, J., Cruz, A.J., Rubio-Gimenez, V., Tietze, M.L., Kravchenko, D.E., Arnauts, G., Matavz, A., Wauteraerts, N., Tu, M., Marcoen, K., 2023. Molecular Layer Deposition of Zeolitic Imidazolate Framework-8 Films. Chem. Mater. 35(4), 1684-1690.
- Stassen, I., Styles, M., Grenci, G., Gorp, H.V., Vanderlinden, W., Feyter, S.D., Falcaro, P., Vos, D.D., Vereecken, P., Ameloot, R., 2016. Chemical vapour deposition of zeolitic imidazolate

- framework thin films. Nat. Mater. 15(3), 304-310.
- Tanskanen, A., Karppinen, M., 2018. Iron-terephthalate coordination network thin films through in-situ atomic/molecular layer deposition. Sci. Rep. 8(1), 1-8.
- Tu, M., Xia, B., Kravchenko, D.E., Tietze, M.L., Cruz, A.J., Stassen, I., Hauffman, T., Teyssandier, J., De Feyter, S., Wang, Z., 2021. Direct X-ray and electron-beam lithography of halogenated zeolitic imidazolate frameworks. Nat. Mater. 20(1), 93-99.
- Wang, K.Y., Weber, M., Chung, T.-S., 2022. Polybenzimidazoles (PBIs) and state-of-the-art PBI hollow fiber membranes for water, organic solvent and gas separations: A review. J. Mater. Chem. A 10(16), 8687-8718.
- Weber, M., Drobek, M., Rebière, B., Charmette, C., Cartier, J., Julbe, A., Bechelany, M., 2020. Hydrogen selective palladium-alumina composite membranes prepared by Atomic Layer Deposition. J. Membr. Sci. 596, 117701.
- Wei, Y., Pastuovic, Z., Shen, C., Murphy, T., Gore, D.B., 2020. Ion beam engineered graphene oxide membranes for mono-/di-valent metal ions separation. Carbon 158, 598-606.
- White, L.S., Amo, K.D., Wu, T., Merkel, T.C., 2017. Extended field trials of Polaris sweep modules for carbon capture. J. Membr. Sci. 542, 217-225.
- Woo, Y.C., Chen, Y., Tijing, L.D., Phuntsho, S., He, T., Choi, J.-S., Kim, S.-H., Shon, H.K., 2017. CF₄ plasma-modified omniphobic electrospun nanofiber membrane for produced water brine treatment by membrane distillation. J. Membr. Sci. 529, 234-242.
- Wu, A.X., Drayton, J.A., Smith, Z.P., 2019. The perfluoropolymer upper bound. AIChE J. 65(12), e16700.
- Xie, K., Fu, Q., Xu, C., Lu, H., Zhao, Q., Curtain, R., Gu, D., Webley, P.A., Qiao, G.G., 2018. Continuous assembly of a polymer on a metal—organic framework (CAP on MOF): A 30 nm thick polymeric gas separation membrane. Energy Environ. Sci. 11(3), 544-550.
- Xu, X., Dolveck, J., Boiteux, G., Escoubes, M., Monchanin, M., Dupin, J., Davenas, J., 1995. Ion beam irradiation effect on gas permeation properties of polyimide films. J. Appl. Polym. Sci. 55(1), 99-105.
- Yang, H., Chen, G., Cheng, L., Liu, Y., Cheng, Y., Yao, H., Liu, Y., Liu, G., Jin, W., 2023. Manipulating gas transport channels in graphene oxide membrane with swift heavy ion irradiation. Sep. Purif. Technol. 320, 124136.
- Ye, J., Zhang, B., Gu, Y., Yu, M., Wang, D., Wu, J., Li, J., 2019. Tailored graphene oxide membranes for the separation of ions and molecules. ACS Appl. Nano Mater. 2(10), 6611-6621.
- Yuan, Z., He, G., Faucher, S., Kuehne, M., Li, S.X., Blankschtein, D., Strano, M.S., 2021. Direct chemical vapor deposition synthesis of porous single-layer graphene membranes with high gas permeances and selectivities. Adv. Mater. 33(44), 2104308.
- Zhang, G., Lin, H., 2023. Indispensable gutter layers in thin-film composite membranes for carbon capture. Green Energy Environ. In press.
- Zhang, G., Tran, T.N., Huang, L., Deng, E., Blevins, A., Guo, W., Ding, Y., Lin, H., 2022. Thin-film composite membranes based on hyperbranched poly(ethylene oxide) for CO₂/N₂ separation. J. Membr. Sci. 644, 120184.

- Zhao, D., Wu, Y., Ren, J., Li, H., Qiu, Y., Deng, M., 2019. Improved CO₂ separation performance of composite membrane with the aids of low-temperature plasma treatment. J. Membr. Sci. 570, 184-193.
- Zhu, L., Huang, L., Venna, S.R., Blevins, A., Ding, Y., Hopkinson, D., Swihart, M.T., Lin, H., 2021. Scalable Polymeric Few-Nanometer Organosilica Membranes for Pre-Combustion CO₂ Capture. ACS Nano 15(7), 12119-12128.
- Zhu, L., Swihart, M.T., Lin, H., 2018. Unprecedented Size-Sieving Ability in Polybenzimidazole Doped with Polyprotic Acids for Membrane H₂/CO₂ Separation. Energy Environ. Sci. 11(1), 94-100.